IEEE Access
Multidisciplinary | Rapid Review | Open Access Journal

Received March 28, 2021, accepted April 3, 2021, date of publication April 7, 2021, date of current version April 16, 2021.

Digital Object Identifier 10.1109/ACCESS.2021.3071477

Mitigation of Derivative Kick Using Time-Varying Fractional-Order PID Control

ATTILA LENDEK, (Student Member, IEEE), AND LIZHE TAN, (Senior Member, IEEE)
Department of Electrical and Computer Engineering, Purdue University Northwest, Hammond, IN 46323, USA
Corresponding authors: Attila Lendek (alendek@pnw.edu) and Lizhe Tan (lizhetan@pnw.edu)

ABSTRACT In this paper, a novel approach for the design of a fractional order proportional integral derivative (FOPID) controller is proposed. This design introduces a new time-varying FOPID controller to mitigate a voltage spike at the controller output whenever a sudden change to the setpoint occurs. The voltage spike exists at the output of the proportional integral derivative (PID) and FOPID controllers when a derivative control element is involved. Such a voltage spike may cause a serious damage to the plant if it is left uncontrolled. The proposed new FOPID controller applies a time function to force the derivative gain to take effect gradually, leading to a time-varying derivative FOPID (TVD-FOPID) controller, which maintains a fast system response and significantly reduces the voltage spike at the controller output. The time-varying FOPID controller is optimally designed using the particle swarm optimization (PSO) or genetic algorithm (GA) to find the optimum constants and time-varying parameters. The improved control performance is validated through controlling the closed-loop DC motor speed via comparisons between the TVD-FOPID controller, traditional FOPID controller, and time-varying FOPID (TV-FOPID) controller which is created for comparison with all three PID gain constants replaced by the optimized time functions. The simulation results demonstrate that the proposed TVD-FOPID controller not only can achieve 80% reduction of voltage spike at the controller output but also is also able to keep approximately the same characteristics of the system response in comparison with the regular FOPID controller. The TVD-FOPID controller using a saturation block between the controller output and the plant still performs best according to system overshoot, rise time, and settling time.

INDEX TERMS Fractional order PID, time-varying derivative FOPID, time-varying FOPID, derivative kick mitigation, particle swarm optimization, genetic algorithm.

NOMENCLATURE

DC	Direct current
DNA	Deoxyribonucleic acid
FOMCON	Fractional-order modeling and control
FOPI	Time invariant fractional order proportional integral
FOPI-D	Fractional-order proportional integral-derivative
FOPID	Time invariant fractional order proportional integral derivative
GA	Genetic algorithm
I-PD	Integral - proportional derivative
IAE	Integral of multiplied absolute error
ISE	Integral of multiplied squared error
ITAE	Integral of time multiplied by absolute error
ITSE	Integral of time multiplied by square error
PI-PD	Proportional integral - proportional derivative
PID	Proportional integral derivative
PMDC	Permanent magnet direct current
PSO	Particle swarm optimization
TV-FOPID	Time-varying fractional order proportional integral derivative
TVD-FOPID	Time-varying derivative fractional order proportional integral derivative
R_a	Armature resistance (Ω)
L_a	Armature inductance (H)
J	Rotor inertia ($Kg \cdot m^2$)
B	Friction constant ($\frac{N \cdot m}{rad/s}$)
k_T	Torque constant ($\frac{N \cdot m}{A}$)
k_e	Electromotive force constant ($\frac{V}{rad/s}$)

The associate editor coordinating the review of this manuscript and approving it for publication was Mohammad Alshabi.

i_a	Armature current (A)
i_f	Field current (A)
T_{em}	Torque ($N \cdot m$)
ω	Rotor angular speed (rad/s)
e_a	Armature voltage (V)
e_b	Back electromotive force (V)

I. INTRODUCTION

A traditional proportional integral derivative (PID) controller is one of the most used type of controller in industrial applications, because it provides stability and rapid responses, for a wide range of operating conditions [1]. The traditional PID has only three controller parameters: proportional gain constant (K_P), integral gain constant (K_I), and derivative gain constant (K_D). The tuning of these parameters is classified as traditional or intelligent methods. The traditional methods like the Ziegler-Nichols [1] do not provide the best tuning. To achieve optimal turning, the use of intelligent methods such as the genetic algorithm (GA) is needed [1]–[9]. The GA is based on genetics and natural evolution, and it mimics the properties of natural selection. Elements generated by the GA are analogous to the chromosome found in deoxyribonucleic acid (DNA). The algorithm searches for the most suitable chromosomes that will successfully build the population in the required solutions space. There has to be a balance between the expansion of the search space and the best solution. Each particle from the selected population of the GA corresponds to a solution to the optimization of the PID parameters. The traditional PID controller has been used for many years now. Most literatures are focused on the controlling aspect of the plant with a reduced error management and not much on the peak values of the control signal leaving the PID controller. There is always a compromise between overshoot, settling time, and the voltage spike, called the derivative kick, coming from the derivative control from the PID controller [10]–[12]. This voltage spike can be attributed to sudden changes to the setpoint, which will give rise to an impulse signal coming from the controller output. The output signal coming from the controller is then fed to control elements such as: electric motors, electronics or control valves, which may be damaged by such sudden high voltage spikes. To mitigate this derivative kick, several researchers have applied the parallel controller structures such as the PI-PD [10], I-PD [11], [12], and the most recent fractional-order proportional integral-derivative (FOPI-D) controller [13]. The PI-PD controller design provides a good overall control of unstable and resonant system's responses to setpoint changes. The I-PD is used to control unstable systems successfully. However, just as the PI-PD controller design, the I-PD controller does not solely target elimination of the derivative or proportional kick. Instead, the elimination of the derivative kick is considered more as a byproduct of the design. As for the FOPI-D [13], it breaks up the controller in order to tackle the derivative kick by placing the derivative block in the feedback path, leading to a change of the control system characteristics.

The fractional order proportional integral derivative (FOPID) has been drawn attention with its advantages over the traditional PID controller. The integral and derivative components in the FOPID controller use fractional integral and derivative calculus [14], [15]. The traditional design methods of FOPID controllers in time-domain and frequency domain can be found in [16]. This way, the FOPID controller ends up with five controller parameters: K_p, K_i, K_d, and the fractional components: order of fractional integration of λ and order of the fractional derivative of μ [16]–[21]. The FOPID controllers provide better energy efficiency in controls [22]. Because the fractional operator has memory, it uses past states to decide on the filtering action, making the control of the plant more efficient. Also, it does provide a more flexible control than the traditional PID controller by allowing the adjustments of the gain and phase characteristics with the help of the fractional components. Such flexibility offered by the FOPID controller is significant for drives such as permanent magnet direct current motors (PMDC). DC motors are usually used in applications that require constant speed, or adjustable speed drives. There are two major types of DC motors: the self-excited and the externally excited ones. The DC motor model used in this paper is an externally excited motor whose speed control is achieved via voltage control applied at the armature. The mathematical model of the DC motor used as the plant can be found in [23]–[29]. The optimal design with the intelligent algorithms is generally employed for FOPID design. Besides the genetic algorithm discussed previously, another popular algorithm is the particle swarm optimization. The particle swarm optimization (PSO) is a population based scholastic optimization technique that mimics swarm intelligence such as school of fish or bird flock; and it does not rely on the survival of the fittest value [9], [30]–[38]. Each individual particle from the swarm moves at certain speed in the search space; and it records its best position in its memory. The best position reached is compared to the best global position; and if it is better than the current global position, then the global position will be updated with that value, which tends to accelerate the search for the global value.

The optimization design techniques used by the PSO and GA need an objective function for optimization. There are four single variable objective functions: integral of time multiplied absolute error (ITAE), integral of absolute error (IAE), integral of time multiplied squared error (ITSE), and the integral of squared error (ISE) [23], [31], [32], [34], [39]. Among these four objective functions, the ITAE yields less settling and rise times with comparable overshoot [23], [31], [34], [39]. The DC motor speed control is one area of focus in our study. In general, the FOPID controller designed using optimization techniques offers better control performance over the generic PID controller.

However, although the FOPID controller using extra parameters does provide better control of the DC motor speed, the derivative kick exists whenever a sudden change to

the setpoint occurs [5], [40], [41]. Again, placing the derivative block in the feedback path reported in [13] is a technique to tackle the derivative kick, but it changes the overall system transfer function, which is not desired. Therefore, there is room to develop a novel approach. The motivation in our research is to force the derivative gain constant in the FOPID controller to take effect gradually, by weighting it using an optimized time function, while maintaining the controlled system output as close as possible to the regular FOPID controller. Note that applying the time-varying FOPID controller does not have total control over the spike, but definitely has a positive impact.

The contributions of the paper are listed below:

1. In this research, time-varying fractional order PID controllers are developed with a purpose to mitigate the derivative kick which exhibits at the controller output in the form of a voltage spike.
2. A particle swarm optimization algorithm is modified to perform the optimal design for the proposed time-varying derivative FOPID (TVD-FOPID) controller and time-varying FOPID (TV-FOPID) controller.
3. Validation of the proposed TVD-FOPID controller is performed through the evaluation of performance indices of different configurations. As a result, the TVD-FOPID controller outperforms the regular FOPID controller. With nearly the same performance indices, the TVD-FOPID offers 80% reduction to the control voltage spike.

The paper is organized as follows. Section II introduces the preliminary concepts, where the basic definitions of the fractional calculus are presented. Section III describes the design of regular time-invariant FOPID controllers. Section IV depicts the derivative kick problem, where the time invariant controllers generate a large spike in the output control voltage whenever a sudden change in the setpoint occurs. Section V presents the structure of the proposed TVD-FOPID and TV-FOPID controllers, which are achieved by optimal design using the PSO as well as GA algorithms to mitigate the voltage spike at the controller output. Section VI illustrates the design of the TVD-FOPID and TV-FOPID controllers for DC motor speed control, and the performance evaluations with different configurations. Section VII presents the conclusions.

II. PRELIMINARY CONCEPTS BASIC DEFINITIONS FOR FRACTIONAL CALCULUS

In the realm of elementary calculus [19], a differentiation operator for the first derivative is defined as $D = \frac{d}{dx}$ and the n^{th} derivative is defined as $D^n f(x) = \frac{d^n f(x)}{dx^n}$, where n is a positive integer. The question from L'Hopital, back in 1695, towards Leibniz was about the meaning of $D^n f(x)$, when n is a fraction such as $n = 1/2$, instead of a positive integer. To which, Leibniz responded: "Thus it follows that will be equal to $d^{0.5}f(x)/dx^{0.5}$, an apparent paradox, from which one day useful consequences will be drawn." [18], [42]. Fractional Calculus is a branch of mathematical analysis where the differentiation and integration are generalized to non-integer order fundamental operator ${}_aD_t^\alpha$. One of the generalized forms of the differ-integrator [5] can be represented as:

$$ {}_aD_t^\alpha f(t) = \frac{d^\alpha f(t)}{[d(t-a)]^\alpha} \tag{1}$$

where a and t are the limits of the operation, α represents the real order of the differ-integral, and $\alpha \in R$. Since a represents the lower limit, it is considered to be zero if not stated and it will not be represented.

The continuous differ-integrator from Equation (1), [7], [8], [14], [19], [26], [27], [37], [41], [43], [44], can be defined below:

$$ {}_aD_t^\alpha \cong D^\alpha = \begin{cases} \frac{d^\alpha}{dt^\alpha} & \alpha > 0, \\ 1 & \alpha = 0, \\ \int_a^t (dt)^{-\alpha} & \alpha < 0. \end{cases} \tag{2}$$

There are multiple definitions of the fractional order operator. The most frequently used general definitions are:

1. The Grunwald-Letnikov (GL) definition [6]–[8], [18], [19], [27], [37], [41]–[45]

$$ {}_aD_t^\alpha f(t) = \lim_{h\to 0} h^{-\alpha} \sum_{j=0}^{\left[\frac{t-a}{h}\right]} (-1)^j \binom{\alpha}{j} f(t-jh), \tag{3}$$

where [.] is a flooring operator or integer part, h is the time step, and $\binom{\alpha}{j} = \frac{\Gamma(\alpha+1)}{\Gamma(j+1)\Gamma(\alpha-j+1)}$, where Γ represents Euler's Gamma function [8], [18], [27].

2. Riemann-Liouville (RL) definition of the fractional-order derivative [7], [13], [14], [34], [41]–[43], [45]

$$ {}_aD_t^\alpha f(t) = \frac{d^\alpha}{dt^\alpha} f(t) = \frac{1}{\Gamma(\mathrm{n}-\alpha)} \frac{d^n}{dt^n} \int_a^t \frac{f(\tau)}{(t-\tau)^{\alpha-n+1}} d\tau, \tag{4}$$

the fractional-order integral [6], [13], [14], [29], [42]

$$ {}_aD_t^{-\alpha} f(t) = {}_aI_t^\alpha f(t) = \frac{1}{\Gamma(\alpha)} \int_a^t (t-\tau)^{\alpha-1} f(\tau) d\tau, \tag{5}$$

for $(n-1 < \alpha < n)$, and Γ represents Euler's Gamma function.

3. M. Caputo definition [6], [7], [18], [29], [42], as a continuous function

$$ {}_aD_t^\alpha f(t) = \frac{1}{\Gamma(\alpha-n)} \int_a^t \frac{f^n(\tau)}{(\mathrm{t}-\tau)^{\alpha-n+1}} d\tau, \tag{6}$$

for $(n-1 < \alpha < n)$.

Euler's Gamma function of $\Gamma(\mathrm{n})$ is defined for all complex numbers, excluding the negative integer numbers, and it is an extension of the factorial function if its argument is represented as:

$$ \Gamma(n) = (n-1)! \tag{7}$$

where n is the positive integer number.

To find the equivalent transfer function of a system from its differential form to the frequency domain or Laplace domain, zero initial conditions are considered. A general form of the Laplace transform of the fractional order derivative, according to [8], [14], [27], [43]–[45], is given by:

$$LD^{\pm\alpha} f(t) = s^{\pm\alpha} \cdot F(s) \tag{8}$$

Equation (8) is useful in calculating the inverse Laplace of the elementary transfer functions such as s^{α} and $s^{-\alpha}$, where α is a positive real number.

III. FRACTIONAL ORDER PROPORTIONAL INTEGRAL DERIVATIVE CONTROLLER $PI^{\lambda}D^{\mu}$

Using the Laplace domain, the construction of a closed loop FOPID system is presented next. Fig.1 depicts a closed loop control system with a FOPID controller. The FOPID controller can be considered as an extension of the traditional PID controllers and is less sensitive to changes of its parameters.

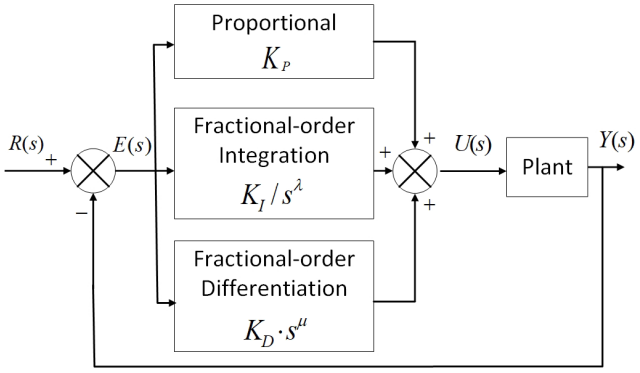

FIGURE 1. Fractional Order PID control closed loop.

A general form of the controller in Laplace domain is given as [5]–[8], [26], [27], [37], [43], [44]:

$$C(s) = \frac{U(s)}{E(s)} = K_p + \frac{K_I}{s^{\lambda}} + K_D s^{\mu} \text{ with } \lambda, \mu \in [0, 2] \tag{9}$$

where $U(s)$ is the control signal, $E(s)$ is the error signal, K_p, K_I, and K_D are the proportional, integral, derivative constant gains, respectively; while λ and μ denote the fractional components: the order of fractional integration and order of the fractional derivative.

In the case of the traditional PID controller as shown in Fig. 2 in the FOPID plane, the values of the fractional components can take combinations of zero or one [6], [18], [31], [43]. In this way, the PID plane consists only of four of points:

if $\lambda = 1$ and $\mu = 1$ then it's a PID controller
if $\lambda = 1$ and $\mu = 0$ then it's a PI controller
if $\lambda = 0$ and $\mu = 1$ then it's a PD controller
if $\lambda = 0$ and $\mu = 0$ then it's a P controller

In the case of the FOPID [18], again as shown in Fig. 2, the values of λ and μ can take any values in the interval $\lambda, \mu \in [0, 2]$. Instead of jumping between points for certain fixed values like in the case of the integer order PID controller,

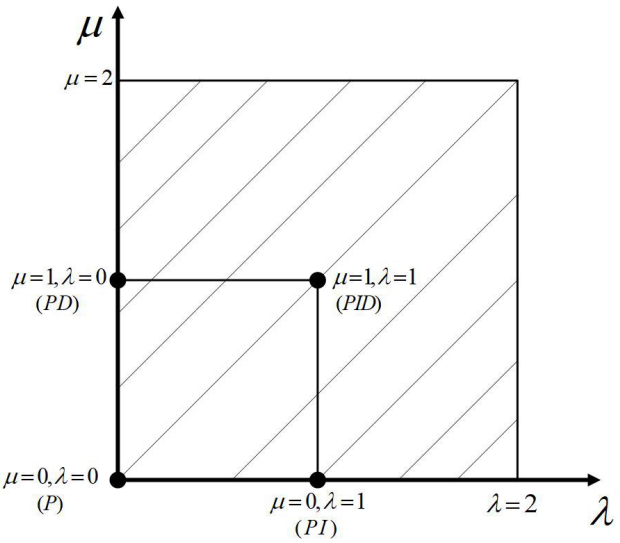

FIGURE 2. Fractional PID controller area.

the fractional components allow continuous movement in the FOPID plane, which is proven to be useful for improving the closed loop control performance [32].

IV. DERIVATIVE KICK PROBLEM

Although the FOPID controller [14], [17]–[21], [32] depicted in Fig. 1 is proven to be useful in improving the closed loop control performance, there exists a general problem caused by the derivative kick, that is, an instant response of the controller that generates a huge spike in the designed control signal $U(s)$ for a step input command. Even though, many researches focus on the improvement of overshoot and settling time [10]–[12] on FOPID controller design, the spike in the control signal is often overlooked. Such a spike is harmful to the control systems and may result in damage to the system devices. To improve overall control system performance, the effect of derivative kick must be investigated. In our research, this aspect of the voltage spike mitigation in the control signal is attempted by designing a time-varying derivative FOPID (TVD-FOPID) controller. This TVD-FOPID controller initially does null the effect of the derivative portion of the controller and then gradually allows for the derivative portion to take its action. The structure of this proposed TVD-FOPID controller is presented in the following section.

V. PROPOSED TIME-VARYING FOPID CONTROLLERS

In this section, we will propose the structure of new time-varying FOPID controllers and illustrate the optimal design methods.

A. THE STRUCTURE OF TIME-VARYING FOPID CONTROLLER

A proposed framework for a closed loop control system using a time-varying FOPID controller is depicted in Fig. 3.

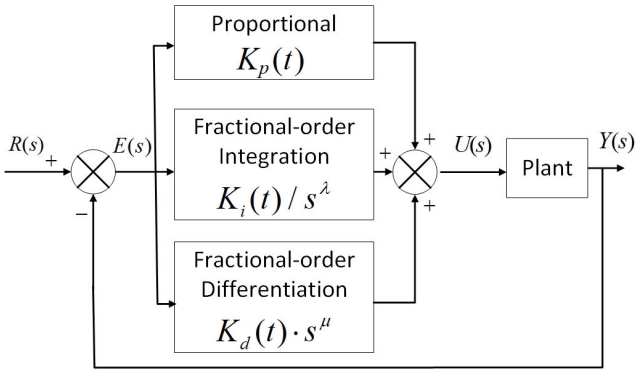

FIGURE 3. Time-varying Fractional Order PID control closed loop.

This structure presents the general case. From this general case, three FOPID controllers are investigated: regular time-invariant controller, proposed time-varying derivative controller and time-varying controller, which are defined below:

1. Regular time-invariant FOPID controller with its five parameters:
   K_P, K_I, K_D, λ and μ
2. Time-varying Derivative FOPID (TVD-FOPID) controller with the following six parameters:
   K_P, K_I, K_D, α_D, λ and μ
3. Time-varying FOPID (TV-FOPID) controller with the following eight parameters:
   K_P, K_I, K_D, α_P, α_I, α_D, λ and μ

As it can be seen, the constants of K_P, K_I, and K_D from the traditional FOPID controller depicted in Fig. 1 are changed to be time-varying functions, that is,

$$K_p(t) = K_P(1 - e^{-\alpha_P t}), \quad t \geq 0 \tag{10}$$

$$K_i(t) = K_I(1 - e^{-\alpha_I t}), \quad t \geq 0 \tag{11}$$

$$K_d(t) = K_D(1 - e^{-\alpha_D t}), \quad t \geq 0 \tag{12}$$

where K_P, K_I, and K_D are the gain parameters, while α_P, α_I, and α_D are the time constants for the fractional-proportional, integral, and derivative controls, respectively. These six parameters along with λ and μ can be designed using optimization algorithms as proposed in the next section.

B. OPTIMAL DESIGN WITH PARTICLE SWARM OPTIMIZATION ALGORITHM

The particle swarm optimization is a global optimization technique that mimics the behavior of schools of fish or flock of birds traveling [30], [33]. Each individual unit in the swarm moves with a dynamically adjusted velocity in the search space based on its own and the swarm group's experience [34], [35]. The memory of each unit holds the information about the best position that it traveled through and this fitness value is stored in *pbest*. There is another value that is kept, the *gbest*, which represents the best overall value and its location achieved by any of the particles from the swarm throughout the search. At each instance of time, the PSO algorithm adjusts the velocity of each individual particle towards its own *pbest* as well as towards the global *gbest*. If a new *pbest* is reached, it will be compared to the *gbest* position. Again, if this new *pbest* is better than the global *gbest*, then the global position will be updated with that value. This tends to accelerate the global value towards a global optimum solution [32]. At the beginning of the setup, a group of particles are initialized in the search space with dimension. The position of the i^{th} particle is given by $X_i = [X_{i1}, X_{i2}, \ldots, X_{iD}]$ and its velocity is given by $V_i = [V_{i1}, V_{i2}, \ldots, V_{iD}]$. The optimal position of a single particle is given by (*pbest*), $P_i = [P_{i1}, P_{i2}, \ldots, P_{iD}]$ and the best global position by (*gbest*) $P_g = [P_{g1}, P_{g2}, \ldots, P_{gD}]$.

The update of the positions and the velocity equations [9], [29], [31], [32], [34], [35], [38] is achieved using Equations (13) and (14), as shown below:

$$V_{id}(t+1) = wV_{id}(t) + c_1 r_1[P_{id} - X_{id}(t)] + c_2 r_2[P_{gd} - X_{id}(t)] \tag{13}$$

$$X_{id}(t+1) = X_{id}(t) + V_{id}(t+1) \tag{14}$$

where

w – inertia weight vector
t – position of current iteration
c_1, c_2 – positive acceleration constants
r_1, r_2 – random numbers in the [0,1] interval.

To overcome a poor velocity control of the particles, a time decreasing inertia [29], [31], [34], [35], [38] is introduced as:

$$w = w_{\max} - \frac{w_{\max} - w_{\min}}{t_{\max}} \cdot t \tag{15}$$

where $w_{\min}$ and $w_{\max}$ are the minimum and maximum of the inertia weight factor, set by the user.

The parameters used in setup of PSO are:
number of variables = 5
number of particles in the swarm = 50
maximum iterations = 30
inertia weight factor minimum $w_{\min} = 0.05$
inertia weight factor maximum $w_{\max} = 0.1$
positive acceleration constants $c_1, c_2 = 2$

The following bounds are set for the controller parameters: $0 \leq K_P \leq 25$, $0 \leq K_I \leq 5$, $0 \leq K_D \leq 5$, $0 \leq \lambda \leq 2$, $0 \leq \mu \leq 1.75$, $0 < \alpha_P < 25$, $0 < \alpha_I < 25$, $0 < \alpha_D < 25$.

To apply the PSO algorithm, an objective function using the integral of time multiplied absolute error (ITAE) is selected. Minimizing the ITAE fitness function [4], [6], [23], [24], [31], [32], [37], [39], [43], [45] through the PSO optimization is a good way to measure the quality of the system at hand [23], [32], meaning that the overshoot, settling time, and rise time are optimized for the transient response of the control system. The ITAE is expressed as

$$ITAE = \int_0^{t_{sim}} t \cdot |e(t)| \cdot dt \tag{16}$$

where t is the time, $|e(t)|$ is the absolute value of the error signal (the difference between the setpoint and the output of

angular speed for DC motor speed control in our study), and t_{sim} is the upper limit of the simulation time.

VI. FOPID CONTROLLER FOR DC MOTOR SPEED CONTROL

To illustrate the proposed method and validate its effectiveness, the time-varying FOPID controller is applied to control the DC motor speed. The DC motor model used in our study is described next.

A. DC MOTOR MODEL

As depicted in Fig. 4, the DC motor model used in this research [1], [9], [23] is an externally excited motor whose speed control is achieved via voltage control applied at the armature e_a.

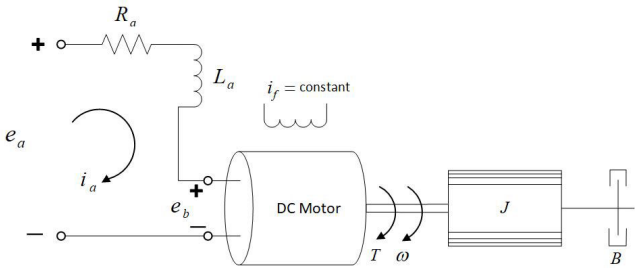

FIGURE 4. Modeling circuit of the DC motor.

At a constant flux, the rotor's angular speed ω in rad/sec is directly proportional to the induced electromotive force e_b [22], [23], that is,

$$e_b = k_e \cdot \omega \tag{17}$$

Modeling the electric circuit around the main loop leads to the following equivalent differential equation for the armature voltage [1], [22], [23]:

$$e_a = L_a \frac{di_a}{dt} + R_a \cdot i_a + e_b \tag{18}$$

The electromagnetic torque produced by the armature current [1], [9], [22], [23] is given by

$$T_{em} = J \frac{d\omega}{dt} + B \cdot \omega = k_T \cdot i_a \tag{19}$$

Since the load torque T_L is an external factor, it is not calculated with the electromagnetic torque. Assuming zero initial conditions, taking Laplace transform of Equations (17)-(19) leads to [23]:

$$E_b(s) = K_e(s) \cdot \omega(s) \tag{20}$$

$$E_a(s) = (L_a \cdot s + R_a) \cdot I_a(s) + E_b(s) \tag{21}$$

$$T_{em}(s) = (J \cdot s + B) \cdot \omega(s) = k_T \cdot I_a(s) \tag{22}$$

Fig. 5 presents the diagram of the open loop transfer function of the DC motor [23], [24].

Through Fig. 5, the transfer function of the DC motor is obtained as

$$G(s) = \frac{\omega(s)}{E_a(s)} = \frac{k_T}{(L_a \cdot s + R_a)(J \cdot s + B) + k_e \cdot k_T} \tag{23}$$

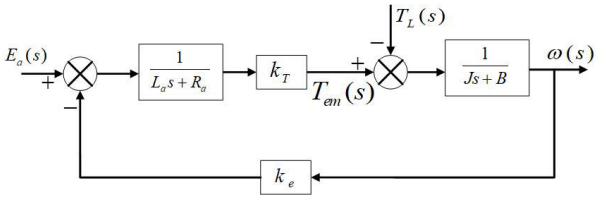

FIGURE 5. DC motor system model.

TABLE 1. Parameters for the DC motor modeling.

Parameters	Values
R_a	0.4 Ω
L_a	2.7 H
J	0.0004 $Kg \cdot m^2$
B	0.0022 $\frac{N \cdot m}{rad/s}$
k_T	0.015 $\frac{N \cdot m}{A}$
k_e	0.05 $\frac{V}{rad/s}$

Table 1 lists the values of the DC motor parameters used in this research.

Substituting the parameter values from Table 1 into Equation (23) yields the following open-loop transfer function:

$$G(s) = \frac{\omega(s)}{E_a(s)} = \frac{0.015}{0.00108 \cdot s^2 + 0.0061 \cdot s + 0.00163} \tag{24}$$

This transfer function representing the plant (DC motor) will be used in our research and implemented in MATLAB/Simulink.

B. FOPID DESIGN

The fractional order controllers are built in MATLAB/Simulink with the fractional order blocks from the fractional-order modeling and control (FOMCON) package [4], [18], [26], [43]–[46]. The FOMCON was developed by Aleksei Tepljakov for the purpose of modeling and controlling of the fractional order dynamic systems. The FOPID design is implemented with the help of MATLAB/Simulink, as depicted in Fig. 6. The R(s) reference is a step input that kicks in at $t = 0$. The response of the closed loop system to the step input is Y(s). The error E(s) is tapped to a set of blocks to obtain the ITAE output, which is then minimized.

The controller configurations and parameter bounds were set below:

Case 1: Regular time-invariant FOPID controller $K_p(t) = K_P$, $K_i(t) = K_I$, $K_d(t) = K_D$ with the following bounds: $0 \le K_P \le 25$, $0 \le K_I \le 5$, $0 \le \lambda \le 2$, $0 \le K_D \le 5$, $0 \le \mu \le 1.75$

Case 2: Time-varying derivative FOPID (TVD-FOPID) controller $K_p(t) = K_P$, $K_i(t) = K_I$, $K_d(t) = K_D(1 - e^{-\alpha_D t})$

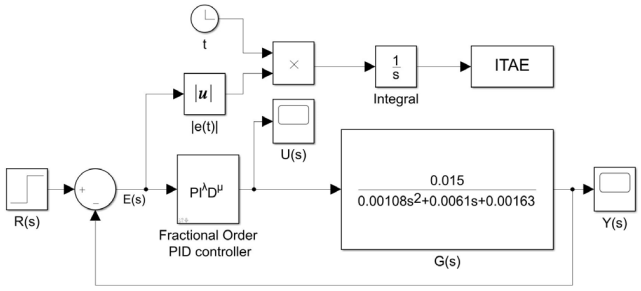

FIGURE 6. FOPID with ITAE in closed loop system.

with the following bounds: $0 \leq K_P \leq 25$, $0 \leq K_I \leq 5$, $0 \leq \lambda \leq 2$, $0 \leq K_d \leq 5$, $0 \leq \mu \leq 1.75$, $0 < \alpha_D < 25$

Case 3: Time-varying FOPID (TV-FOPID) controller $K_p(t) = K_P(1 - e^{-\alpha_P t})$, $K_i(t) = K_I(1 - e^{-\alpha_I t})$, $K_d(t) = K_D(1 - e^{-\alpha_D t})$ with the following bounds: $0 \leq K_P \leq 25$, $0 \leq K_I \leq 5$, $0 \leq \lambda \leq 2$, $0 \leq K_D \leq 5$, $0 \leq \mu \leq 1.75$, $0 < \alpha_P < 25$, $0 < \alpha_I < 25$, $0 < \alpha_D < 25$.

Fig. 6 shows the Simulink model of the closed loop regular time-invariant FOPID controller with the ITAE objective function.

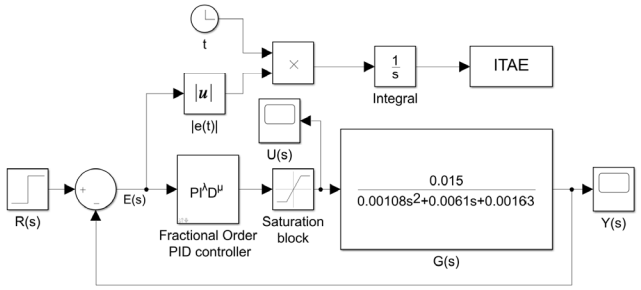

FIGURE 7. FOPID with ITAE in closed loop system with saturation block.

Fig. 7 Illustrates the Simulink model of the closed loop time-invariant FOPID controller with the ITAE objective function and an additional saturation unit. The control signal is limited as $|u(t)| < 12\ V$.

Running the PSO and GA optimization algorithms on the above setups, the convergence curves are obtained for both linear and non-linear configurations. Fig. 8 shows ITAE values obtained by the PSO, while Fig.9 depicts the ITAE values obtained by GA.

As shown in Figs. 8 and 9, it is observed that the PSO optimization offers lower errors as well as the lower computational complexity. The optimization parameters from both PSO and GA algorithms are listed in Table 2 for the linear configuration without using a saturation block and Table 3 for the nonlinear configuration with a saturation block.

Table 2 details the parameter values found by PSO and GA, including the time constants and the fractional order of operators for the case of the linear controllers.

Table 3 details the parameter values found by PSO and GA, including the time constants and the fractional order

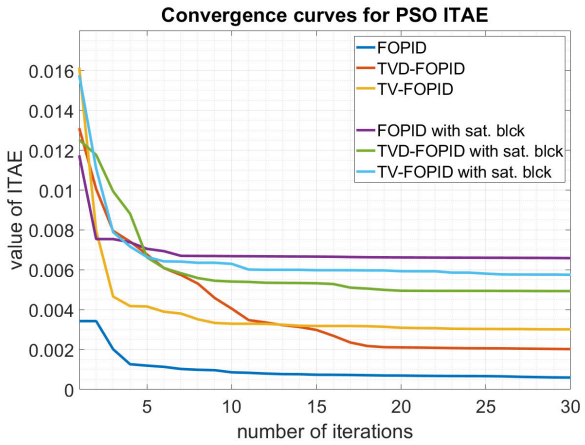

FIGURE 8. Convergence curves for PSO using ITAE, without and with saturation block.

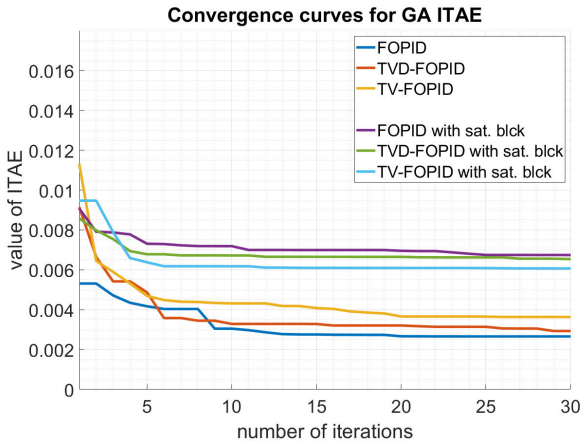

FIGURE 9. Convergence curves for GA using ITAE, without and with saturation block.

TABLE 2. Parameter values for controllers without saturation block.

Algorithm	K_p, K_i, K_d		λ, μ
PSO FOPID	19.499,5.000,3.379		1.020, 1.004
PSO TVD-FOPID	15.673,3.424,5.000	α_D	1.103, 1.154
		25.000	
PSO TV-FOPID	21.294,3.585,2.256	$\alpha_P, \alpha_I, \alpha_D$	1.002, 0.999
		8.575,17.093,19.677	
GA FOPID	23.952,3.472,3.323		1.39, 1.151
GA TVD-FOPID	19.402,3.437,4.996	α_D	1.273, 1.278
		24.077	
GA TV-FOPID	18.997,3.603,2.967	$\alpha_P, \alpha_I, \alpha_D$	1.015, 1.022
		8.389,13.144,9.635	

operators, for the case of the nonlinear controllers with a saturation block. After obtaining the optimized parameters, the step responses and the control voltage spikes are compared for evaluation.

TABLE 3. Parameter values for controllers with saturation block.

Algorithm	K_p, K_i, K_d		λ, μ
PSO FOPID	25.000,2.336,2.453		0.664, 0.827
PSO TVD-FOPID	17.161,1.352,3.354	α_D	0.961, 0.955
		8.443	
PSO TV-FOPID	24.999,3.138,2.949	$\alpha_P, \alpha_I, \alpha_D$	1.002, 0.977
		5.571,9.178,6.803	
GA FOPID	24.839,1.942,1.795		0.757, 0.902
GA TVD-FOPID	19.114,2.58,3.457	α_D	0.615, 0.827
		16.938	
GA TV-FOPID	17.131,3.431,3.344	$\alpha_P, \alpha_I, \alpha_D$	0.847, 0.88
		9.17,13.579,8.093	

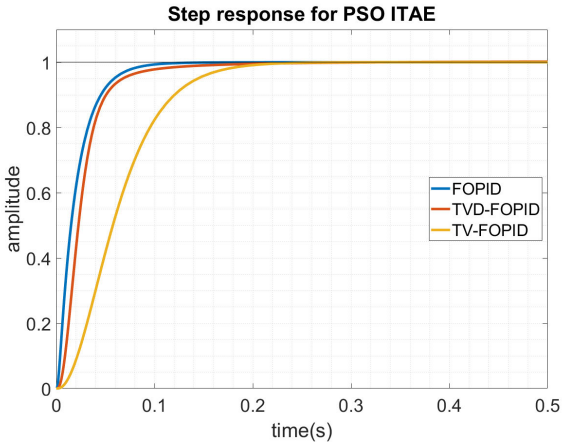

FIGURE 10. Step response for PSO using ITAE.

C. CONTROL PERFORMANCE EVALUATION OF FOPID CONTROLLERS

Fig. 10 shows the step responses of the linear systems, where it is observed that there is no overshoot in any of the presented cases. There is very little difference in the rise time and the settling time between case 1 and case 2, that is, the time-invariant FOPID, and the time-varying derivative FOPID (TVD-FOPID). In fact, the 6-element TVD-FOPID controller achieves almost the same performance as the 5-element time-invariant FOPID controller.

The control voltages of the linear systems, U(s), with the afferent spikes that this research tries to mitigate, are presented in Fig. 11. The most preeminent spike comes from the time-invariant FOPID with maximum at 1300V, which occurs at 1ms. The TVD-FOPID controller only has a maximum value of 260V occurring much later at 3.8ms. Clearly there is an 80% reduction in the derivative kick, with minimal loss in the rise time and the settling time. In addition, the 8-element TV-FOPID has the maximum value of 45V, which occurs at 5.4ms. 96.5% of reduction in the derivative kick is evidenced with a trade-off that comes with longer rise time and settling time.

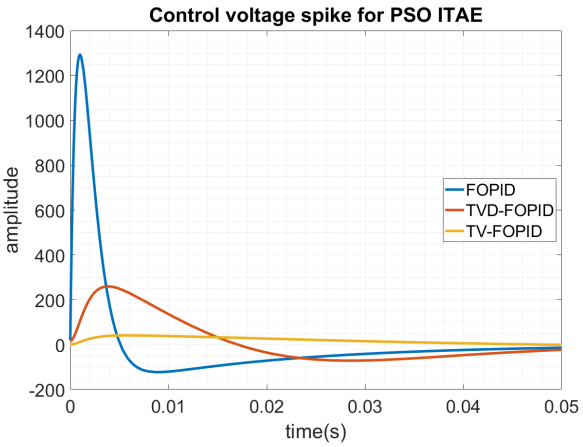

FIGURE 11. Controller output for PSO using ITAE.

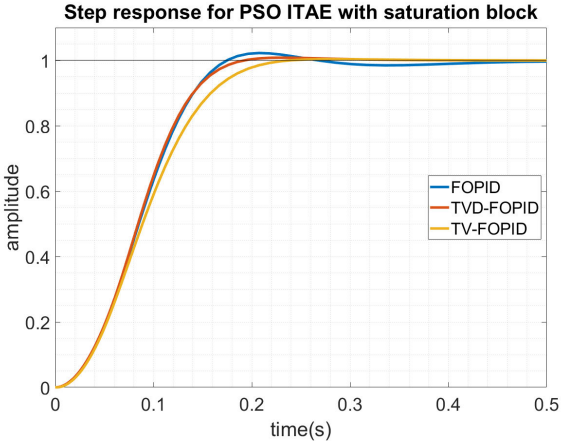

FIGURE 12. Step response for PSO using ITAE with saturation block.

Fig. 12 shows the step responses of the nonlinear systems (saturation unit). It is observed that the TVD-FOPID configuration offers the best control performance in terms of the overshoot, rise time, and settling time.

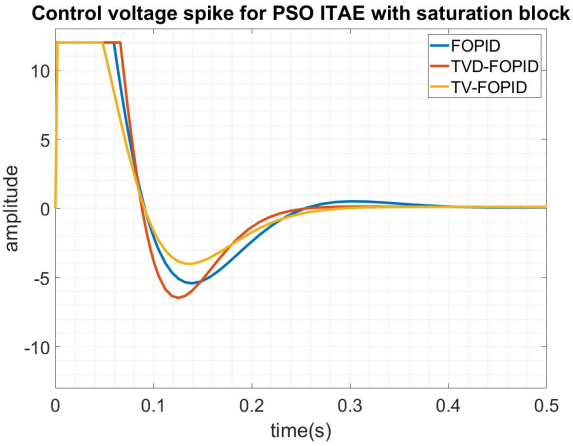

FIGURE 13. Controller output for PSO using ITAE with saturation block.

Fig. 13 shows the control voltages of the nonlinear systems, U(s). As shown in Fig. 13, the TVD-FOPID controller with

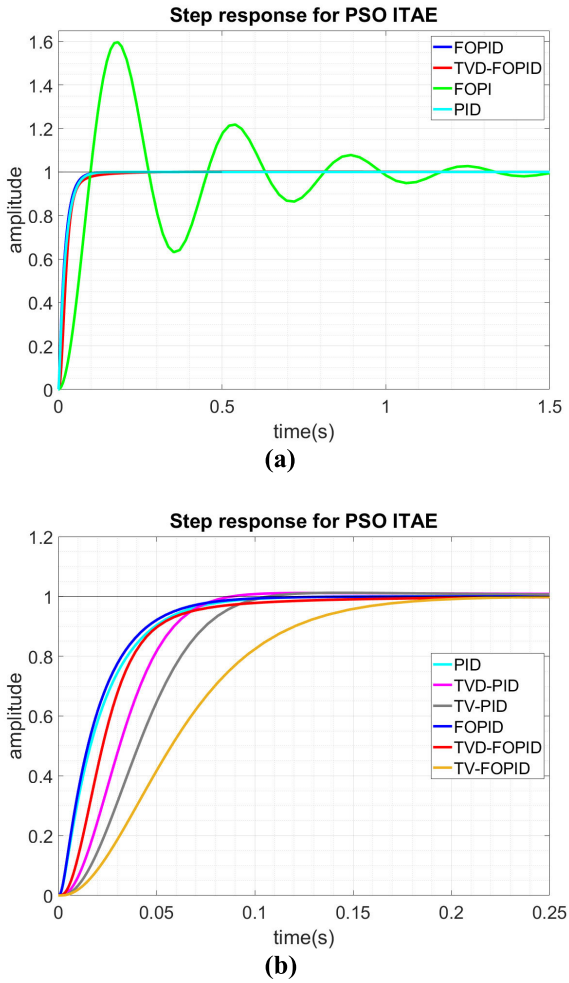

FIGURE 14. Step response for PSO using ITAE.

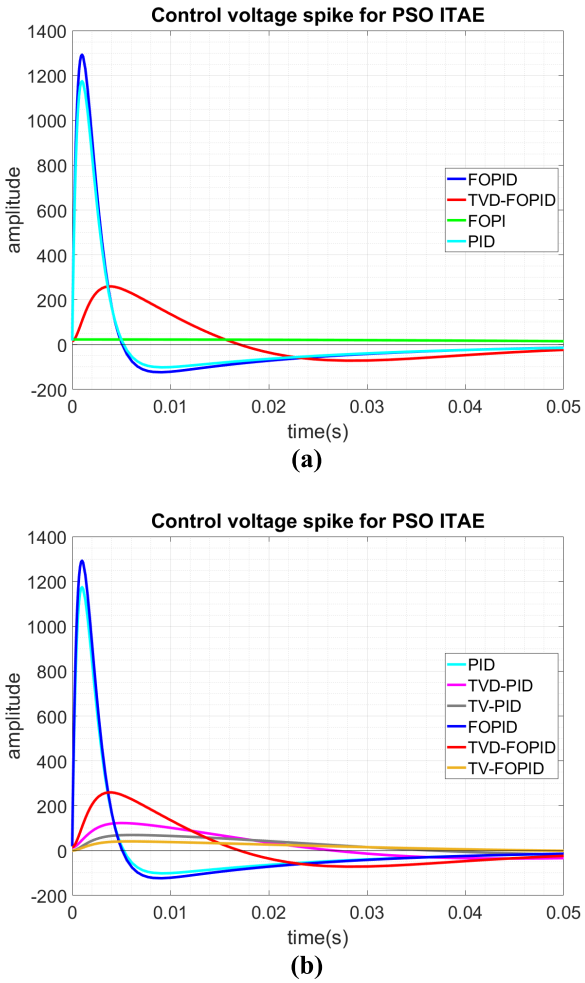

FIGURE 15. Controller output for PSO using ITAE.

the saturation unit takes a little bit more time at saturation level of 12 volts; and it has the largest negative peak. It is clear that all the control signals are well within the practical range $|u(t)| < 12\ V$.

Additional simulations and comparisons were conducted using the developed TVD-FOPID, TV-FOPID, standard FOPID, FOPI (no derivative component), TVD-PID, TV-PID, and genetic PID controllers. Further comparison with the other type of control methods such as the sliding mode control (SMC) method [47], [48] will be our future research work.

The step responses from the developed TVD-FOPID, FOPID, FOPI [49], and PID controllers are displayed in Fig. 14(a). As shown in Fig. 14(a), the responses from the TVD-FOPID, FOPID, and generic PID controllers are similar. However, the response of the FOPI controller has unacceptable overshoot and settling time. Fig 14(b) presents a more comprehensive comparison of step responses from time-varying, non-time varying, fractional-order, and integer-order PID controllers. We can see that besides the TV-FOPID and TV-PID controllers, the TVD-FOPID and FOPID controllers have faster response than the TVD-PID and PID controllers, respectively.

Fig. 15(a) shows the controller voltage outputs from TVD-FOPID, FOPID, FOPI [49], and generic PID controllers. This figure indicates that the voltage spikes from the FOPID and generic PID controllers are similarly high, while the voltage spike from our developed TVD-FOPID controller is reduced by 80% when compared to the FOPID and generic PID controllers. The voltage spike using the FOPI controller is minimal due to the absence of the derivative component. Fig 15(b) shows the controller outputs for all different PID controllers. From Fig. 15 (b), the TVD-PID controller offers more spike reduction in comparison with the TVD-FOPID controller but it is less favorable to the TVD-FOPID controller due its slow response.

The step responses of the nonlinear systems from the developed TVD-FOPID, FOPID, FOPI [49] and PID controllers are presented Fig. 16 (a). As shown in Fig. 16 (a), the responses from our developed TVD-FOPID controller and regular FOPID controller are similarly fast, while the responses from the FOPI and generic PID controllers

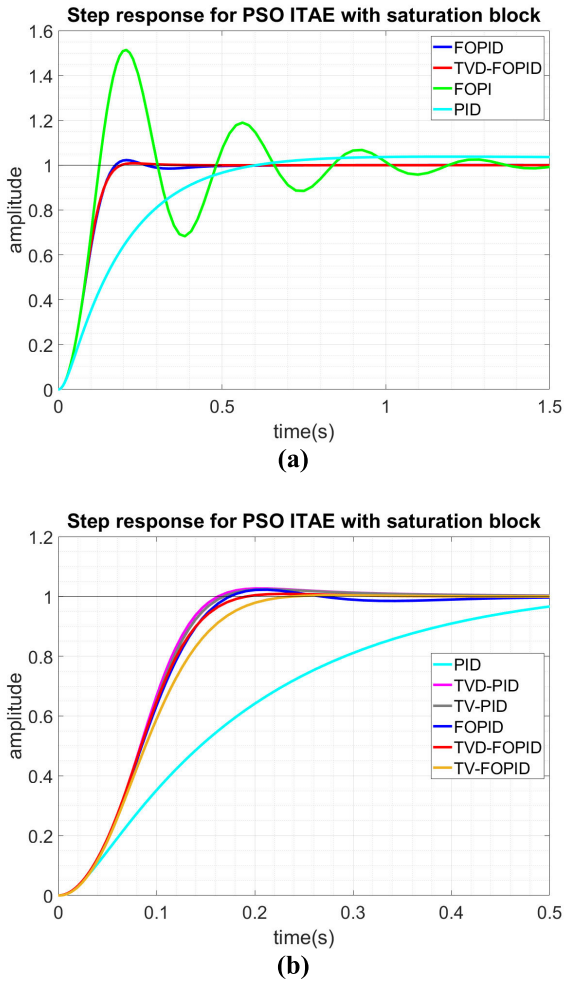

FIGURE 16. Step response for PSO using ITAE with saturation block.

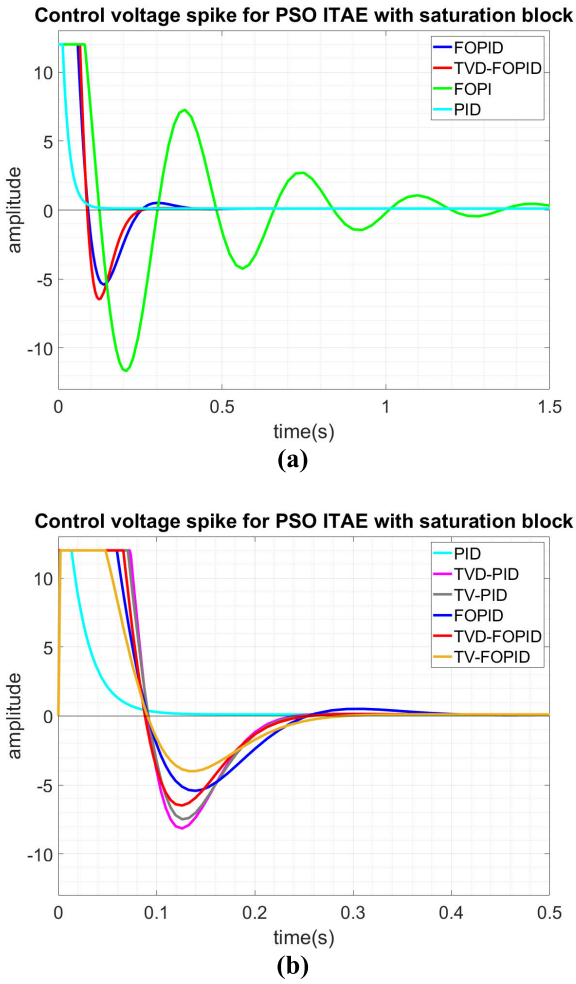

FIGURE 17. Controller output for PSO using ITAE with saturation block.

are sluggish. As shown in Fig. 16 (b) for a comparison of all the PID controllers, the TVD-FOPID, TVD-PID, and FOPID controllers have a high performance. Although TVD-PID and FOPID have quicker rise times, they suffer from the over shoot and longer settling time. Instead, the proposed TVD-FOPID controller offers the best control quality in terms of no overshoot and faster settling time.

Fig. 17(a) depicts the control voltage outputs of the non-linear systems from the developed TVD-FOPID, FOPID, FOPI [49], and PID controllers. It can be observed that the generic PID controller has the shortest saturation time, followed by the FOPID, TVD-FOPID, and lastly, by the FOPI controllers. For the comparison of all the various PID controllers depicted in Fig. 17 (b), it can be seen that besides the generic PID controller, all the controllers spend time in the saturation region. The generic PID controller spends the least amount of time in the saturation region and has no negative spike, but it accommodates an unacceptable settling time, as shown in Fig. 16 (b).

Clearly, our developed TVD-FOPID controller retains the same transient characteristics as the standard FOPID controller but has a significant reduction of voltage spike at the controller output. Furthermore, the TVD-FOPID controller offers faster settling time. For the rest of this paper, the focus is on the FOPID and time-varying FOPID controllers.

D. SPEED CONTROL OF DC MOTOR USING VARIOUS APPROACHES

1) OVERSHOOT, RISE TIME AND SETTLING TIME

To compare the performances from the FOPID, novel TVD-FOPID, and TV-FOPID controllers, the overshoot, rise time, and settling time were measured and gathered in Table 4. From the overshoot prospective there is no significant difference between the compared controllers. When comparing the settling times, the TVD-FOPID controller offers far better settling times than the TV-FOPID controllers.

Table 5 contains the data gathered at the controller output. It provides a comparison between the voltage spike for the case of the linear controller, and the duration of saturation for the case of the nonlinear controller with a saturation block present. For the linear controllers, once again, designed by

TABLE 4. Comparison of the transient response for GA and PSO.

Algorithm	Overshoot	Rise time[ms]	Settling time[ms]
PSO FOPID	0.0%	41.562	77.474
PSO TVD-FOPID	0.2%	41.861	104.611
PSO TV-FOPID	0.4%	121.309	201.879
GA FOPID	0.0%	37.937	152.950
GA TVD-FOPID	0.3%	37.709	122.356
GA TV-FOPID	0.0%	103.160	184.932

TABLE 5. Comparison of spike in the control voltage for PSO and GA controller designs.

Algorithm	Linear controller Spike [V]	Nonlinear controller saturation time [ms]
PSO FOPID	1293	59.66
PSO TVD-FOPID	259.2	66.23
PSO TV-FOPID	40.88	48.05
GA FOPID	3214	55.13
GA TVD-FOPID	483.1	70.48
GA TV-FOPID	30.92	53.19

the PSO does provide roughly 50% lower spikes for both the FOPID and TVD-FOPID, than the ones designed by the GA. When comparing the FOPID to the TVD-FOPID, the latter does offer a reduction of 80% in the voltage spike. When comparing the nonlinear controllers, the best scenario is offered by the controller that will stay the least time in the saturation zone. There is no overall significant difference observed between the various FOPID controllers. The average time is 58.79 ms. It can be concluded that, the PSO TVD-FOPID offers a far superior performance in mitigating the voltage spike, due to the derivative kick, when compared to the other designed controllers.

2) COMPARISON OF PERFORMANCE INDICES

In addition, the integral of time multiplied squared error (ITSE) is also evaluated to compare with the ITAE. The ITSE is also widely used in industry [23], [29], [31], [34], [35], [38], [39], [43], [45] and it is defined below:

$$ITSE = \int_0^{t_{sim}} t \cdot e^2(t)dt \tag{25}$$

where t is the time, $e(t)$ is the error signal (the difference between the setpoint and the angular speed output for DC motor speed control in our study), and t_{sim} is the upper limit of the simulation time. From Table 6, it can be seen that the errors from the PSO design are lower in ITSE index, when compared to the ITAE.

3) FREQUENCY RESPONSE ANALYSIS AND STABILITY

The time-varying system stability and working frequency bandwidth are examined next. As a typical illustration, the frequency response of the PSO TVD-FOIPID is displayed in Fig. 18 since this is the one which offers the most promising

TABLE 6. Comparison of performance indices, for different controllers.

Algorithm	ITAE	ITSE
PSO FOPID	0.000597	0.0000460
PSO TVD-FOPID	0.002024	0.0000748
PSO TV-FOPID	0.003014	0.0002100
GA FOPID	0.002659	0.0000490
GA TVD-FOPID	0.002931	0.0001020
GA TV-FOPID	0.003633	0.0002780

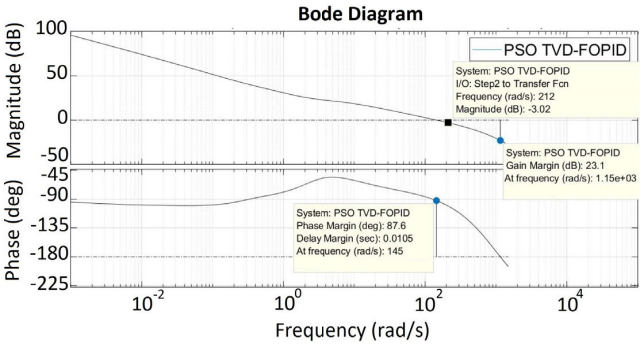

FIGURE 18. Bode plot of PSO TVD-FOPID.

behavior in voltage spike mitigation at the controller output. As it can be seen from Fig. 18, the PSO TVD-FOPID has a gain margin of 23.1 dB, a phase margin of 87.6 degrees, and a frequency bandwidth of 212 rad/sec, which is measured in open-loop gain at -3 dB. Since the gain margin value is much larger than 0 dB and the phase margin is larger than 15 degrees, the final settled TVD-FOPID control system has high relative stability.

TABLE 7. Bode analysis for different controllers.

Algorithm	Gain margin [dB]	Phase margin [deg]	Bandwidth [rad/s]
PSO FOPID	33.1	84.9	67.9
PSO TVD-FOPID	23.1	87.6	212.0
PSO TV-FOPID	36.8	80.3	45.8
GA FOPID	25.4	93.7	134.0
GA TVD-FOPID	17.3	77.5	432.0
GA TV-FOPID	33.4	86.6	64.4

Table 7 lists the gain margin, phase, and bandwidth obtained from the frequency response for each controller, designed by the PSO and GA algorithms. It can be seen that although the gain margins from the optimized TVD-FOPID controllers are relatively low (but much higher than stability requirement of 0 dB), the PSO and GA optimized TVD-FOPID controllers offer three times more bandwidth in comparison with the regular FOPID controllers, implying faster and better transient responses of the developed controller.

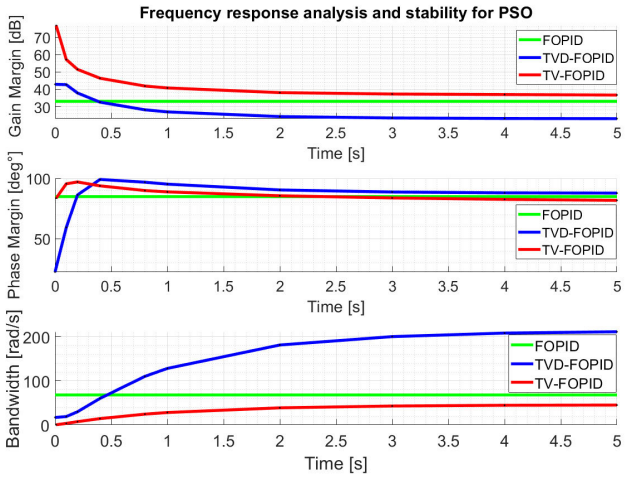

FIGURE 19. PSO gain margin, phase margin, bandwidth for stability.

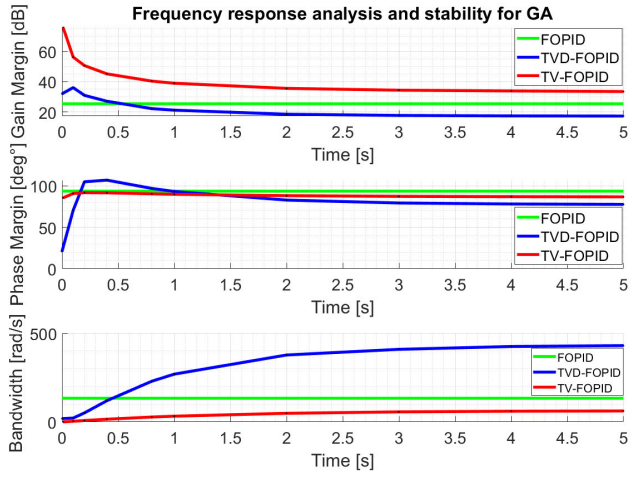

FIGURE 20. GA gain margin, phase margin, bandwidth for stability.

To validate the stability of the TVD-FOPID and TV-FOPID controllers during the time varying period, the frequency response sweep was done for different values of the time instants. Since the FOPID controller is time-invariant, it does remain constants in terms of gain margin, phase margin, and bandwidth, as the green lines shown in Fig. 19 for the PSO optimized controllers and Fig. 20 for the GA optimized controllers. The TVD-FOPID responses for gain margin, phase margin, and bandwidth (blue) were measured at the following time instants (sec): 0, 0.1, 0.2, 0.4, 0.8, 1, 2, 3, 4, 5. As for the PSO TV-FOPID controller, the responses of gain margin, phase margin, and bandwidth (red) were measured at the following time instants(sec): 0.01, 0.1, 0.2, 0.4, 0.8, 1, 2, 3, 4, 5. Note that the first time instant for measurement starts at 0.01 seconds for the PSO TV-FOPID to eliminate the condition that all controller gains are set to zero to begin with.

Based on Table 7, Figs. 19 and 20, it can be concluded that both the linear and nonlinear, and time-invariant and time-varying controllers designed by the PSO or GA exhibit a stable behavior. More specifically, during the time-varying period, the gain margins for the TVD-FOPID and TV-FOPID systems are significantly high initially and then decrease gradually, but are settled to high dB values while their phase margins and bandwidths are gradually improved. Furthermore, the TVD-FOPID controller offers a remarkable improvement on bandwidth.

VII. CONCLUSION

The time-varying derivative fractional order proportional integral derivative (TVD-FOPID) controller has been developed and proposed. The TVD-FOPID controller has a time-varying derivative gain which is achieved via an optimized time function. For a comparison purpose, the time-varying (TV-FOPID) controller with the proportional, integral, and derivative gains which are replaced by the corresponding optimized time functions, respectively, are investigated. Both TVD-FOPID and TV-FOPID controllers have been optimally designed using PSO or GA, based on the regular FOPID controller parameters and time function parameters. The developed TVD-FOPID controller initially suppresses only the effect of the derivative action from the controller, then it takes effect gradually to its full capacity, while the TV-FOPID controller initially suppresses the proportional, integral, and derivative actions, and then the three gains gradually reach their full capacity, in order to ameliorate the effectiveness of the derivative kick. The proposed TVD-FOPID controller has the ability to mitigate the derivative kick by reducing voltage spike at the controller output by a stunning value of 80% while keeping the system overshoot, settling time and rise time on par with the regular FOPID controller. The TV-FOPID controller offers maximum reduction of derivative kick, but it comes with a trade-off in control performance degradation, in terms of the delayed rise time and settling time. The TVD-FOPID controller is validated as the best choice when dealing with mitigation of the derivative kick. The proposed TVD-FOPID controller with a saturation block between the controller output and the plant process is still validated to have the best performance in terms of system overshoot, rise time and settling time. In addition, the time-varying gain margin, phase margin, and bandwidth are also simulated to demonstrate that all controllers designed by the PSO and GA exhibit stable behaviors and feasible working frequency bandwidths. Since our proposed TVD-FOPID controller with optimal design approach is developed as a generic case, it can be applied to any control system in which the derivative kick exists. Our future work will also apply the developed TVD-FOPID controller with optimal design to various practical systems, including hardware validations.

REFERENCES

[1] A. T. El-Deen, A. A. H. Mahmoud, and A. R. El-Sawi, "Optimal PID tuning for DC motor speed controller based on genetic algorithm," *Int. Rev. Autom. Control*, vol. 8, no. 1, pp. 80–85, Jan. 2015.

[2] T. Maruyama and H. Igarashi, "An effective robust optimization based on genetic algorithm," *IEEE Trans. Magn.*, vol. 44, no. 6, pp. 990–993, Jun. 2008, doi: 10.1109/TMAG.2007.916696.

[3] S. Tsutsui and A. Ghosh, "Genetic algorithms with a robust solution searching scheme," *IEEE Trans. Evol. Comput.*, vol. 1, no. 3, pp. 201–208, Sep. 1997, doi: 10.1109/4235.661550.

[4] S. A. Gunawan, Y. C. H. Yuwono, G. N. P. Pratama, A. I. Cahyadi, and B. Winduratna, "Optimal fractional-order PID for DC motor: Comparison study," in *Proc. 4th Int. Conf. Sci. Technol. (ICST)*, Yogyakarta, Indonesia, Aug. 2018, pp. 1–6, doi: 10.1109/ICSTC.2018.8528704.

[5] S. Mehta and M. Jain, "Comparative analysis of different fractional PID tuning methods for the first order system," in *Proc. Int. Conf. Futuristic Trends Comput. Anal. Knowl. Manage. (ABLAZE)*, Noida, India, Feb. 2015, pp. 640–646, doi: 10.1109/ABLAZE.2015.7154942.

[6] J. Wan, B. He, D. Wang, T. Yan, and Y. Shen, "Fractional-order PID motion control for AUV using cloud-model-based quantum genetic algorithm," *IEEE Access*, vol. 7, pp. 124828–124843, 2019, doi: 10.1109/ACCESS.2019.2937978.

[7] N. Radmehr, H. Kharrati, and N. Bayati, "Optimized design of fractional-order PID controllers for autonomous underwater vehicle using genetic algorithm," in *Proc. 9th Int. Conf. Electr. Electron. Eng. (ELECO)*, Nov. 2015, pp. 729–733.

[8] J.-Y. Cao, J. Liang, and B.-G. Cao, "Optimization of fractional order PID controllers based on genetic algorithms," in *Proc. Int. Conf. Mach. Learn. Cybern.*, Guangzhou, China, vol. 9, 2005, p. 5686, doi: 10.1109/ICMLC.2005.1527950.

[9] Jalilvand, A. Kimiyaghalam, A. Ashouri, and H. Kord, "Optimal tuning of PID controller parameters on a DC motor based on advanced particle swarm optimization algorithm," *Int. J. Tech. Phys. Problems Eng.*, vol. 3, no. 4, pp. 10–17, Dec. 2011.

[10] D. P. Atherton and S. Majhi, "Limitations of PID controllers," in *Proc. Amer. Control Conf.*, San Diego, CA, USA, vol. 6, 1999, pp. 3843–3847, doi: 10.1109/ACC.1999.786236.

[11] X. Zhu, "Practical PID controller implementation and the theory behind," in *Proc. 2nd Int. Conf. Intell. Netw. Intell. Syst.*, Tianjin, China, Nov. 2009, pp. 58–61, doi: 10.1109/ICINIS.2009.24.

[12] V. T. Diep, P. D. Hung, and N. T. Su, "I-PD controller design based on robust viewpoint," in *Proc. 2nd Int. Conf. Intell. Robotic Control Eng. (IRCE)*, Singapore, Aug. 2019, pp. 27–31, doi: 10.1109/IRCE.2019.00013.

[13] D. Guha, P. K. Roy, S. Banerjee, S. Padmanaban, F. Blaabjerg, and D. Chittathuru, "Small-signal stability analysis of hybrid power system with quasi-oppositional sine cosine algorithm optimized fractional order PID controller," *IEEE Access*, vol. 8, pp. 155971–155986, 2020, doi: 10.1109/ACCESS.2020.3018620.

[14] A. Neçaibia, F. Abdelliche, S. Ladaci, and A. Bouraiou, "Optimal auto-tuning of fractional order PI^{λ} D^{μ} controller for a DC motor speed using Extremum seeking," in *Proc. Int. Conf. Fractional Differentiation Appl. (ICFDA)*, Catania, Italy, 2014, pp. 1–6, doi: 10.1109/ICFDA.2014.6967429.

[15] Y. Luo and Y. Chen, "Fractional order [proportional derivative] controller for a class of fractional order systems," *Automatica*, vol. 45, no. 10, pp. 2446–2450, Oct. 2009.

[16] C. Monje, Y. Chen, B. Vinagre, D. Xue, and V. Feliu, *Fractional-Order Systems and Controls: Fundamentals and Applications*. London, U.K.: Springer-Verlag, 2010.

[17] Y. Yang, H. H. Zhang, W. Yu, and L. Tan, "Optimal design of discrete-time fractional-order PID controller for idle speed control of an IC engine," *Int. J. Powertrains*, vol. 9, nos. 1–2, p. 79, 2020.

[18] P. Shah and S. Agashe, "Review of fractional PID controller," *Mechatronics*, vol. 38, pp. 29–41, Sep. 2016.

[19] R. Caponetto, G. Dongola, L. Fortuna, and I. Petrá, *Fractional Order Systems: Modeling and Control Applications*. Singapore: World Scientific, 2010.

[20] I. Podlubny, "Fractional-order systems and PI^{λ} D^{μ}-controllers," *IEEE Trans. Autom. Control*, vol. 44, no. 1, pp. 208–214, Jan. 1999, doi: 10.1109/9.739144.

[21] N. Ullah, M. A. Ali, A. Ibeas, and J. Herrera, "Adaptive fractional order terminal sliding mode control of a doubly fed induction generator-based wind energy system," *IEEE Access*, vol. 5, pp. 21368–21381, 2017, doi: 10.1109/ACCESS.2017.2759579.

[22] S. Khubalkar, A. Junghare, M. Aware, and S. Das, "Modeling and control of four quadrant chopper fed DC series motor using two-degree of freedom digital fractional order PID controller," in *Proc. IEEE Transp. Electrific. Conf. (ITEC-India)*, Pune, India, Dec. 2017, pp. 1–5, doi: 10.1109/ITEC-India.2017.8333876.

[23] B. Hekimoglu, "Optimal tuning of fractional order PID controller for DC motor speed control via chaotic atom search optimization algorithm," *IEEE Access*, vol. 7, pp. 38100–38114, 2019, doi: 10.1109/ACCESS.2019.2905961.

[24] A. Ahmed, G. Parmar, and R. Gupta, "Application of GWO in design of fractional order PID controller for control of DC motor and robustness analysis," in *Proc. Int. Conf. Adv. Comput., Commun. Control Netw. (ICACCCN)*, Greater Noida, India, Oct. 2018, pp. 646–651, doi: 10.1109/ICACCCN.2018.8748548.

[25] A. T. Mohamed, M. F. Mahmoud, L. A. Said, and A. G. Radwan, "Design of FOPID controller for a DC motor using approximation techniques," in *Proc. Novel Intell. Lead. Emerg. Sci. Conf. (NILES)*, Giza, Egypt, Oct. 2019, pp. 142–145, doi: 10.1109/NILES.2019.8909339.

[26] S. Chakraborty, S. Roy, and U. Mondal, "Fractional-order controller for the position control of a DC motor," in *Proc. IEEE Appl. Signal Process. Conf. (ASPCON)*, Kolkata, India, Dec. 2018, pp. 1–3, doi: 10.1109/ASPCON.2018.8748544.

[27] J. Viola, L. Angel, and J. M. Sebastian, "Design and robust performance evaluation of a fractional order PID controller applied to a DC motor," *IEEE/CAA J. Automatica Sinica*, vol. 4, no. 2, pp. 304–314, Apr. 2017, doi: 10.1109/JAS.2017.7510535.

[28] R. Duma, P. Dobra, and M. Trusca, "Embedded application of fractional order control," *Electron. Lett.*, vol. 48, no. 24, pp. 1526–1528, Nov. 2012, doi: 10.1049/el.2012.1829.

[29] O. Saleem and F. Abbas, "Nonlinear self-tuning of fractional-order PID speed controller for PMDC motor," in *Proc. 13th Int. Conf. Emerg. Technol. (ICET)*, Islamabad, Pakistan, Dec. 2017, pp. 1–6, doi: 10.1109/ICET.2017.8281661.

[30] J. Kennedy and R. Eberhart, "Particle swarm optimization," in *Proc. Int. Conf. Neural Netw. (ICNN)*, Perth, WA, Australia, vol. 4, 1995, pp. 1942–1948, doi: 10.1109/ICNN.1995.488968.

[31] R. V. Jain, M. V. Aware, and A. S. Junghare, "Tuning of fractional order PID controller using particle swarm optimization technique for DC motor speed control," in *Proc. IEEE 1st Int. Conf. Power Electron., Intell. Control Energy Syst. (ICPEICES)*, Delhi, India, Jul. 2016, pp. 1–4, doi: 10.1109/ICPEICES.2016.7853070.

[32] W. Lin and Z. Chongquan, "Design of optimal fractional-order PID controllers using particle swarm optimization algorithm for DC motor system," in *Proc. IEEE Adv. Inf. Technol., Electron. Autom. Control Conf. (IAEAC)*, Chongqing, China, Dec. 2015, pp. 175–179, doi: 10.1109/IAEAC.2015.7428542.

[33] Y. del Valle, G. K. Venayagamoorthy, S. Mohagheghi, J.-C. Hernandez, and R. G. Harley, "Particle swarm optimization: Basic concepts, variants and applications in power systems," *IEEE Trans. Evol. Comput.*, vol. 12, no. 2, pp. 171–195, Apr. 2008, doi: 10.1109/TEVC.2007.896686.

[34] A. Roy and S. Srivastava, "Design of optimal PI^{λ} D^{μ} controller for speed control of DC motor using constrained particle swarm optimization," in *Proc. Int. Conf. Circuit, Power Comput. Technol. (ICCPCT)*, Nagercoil, India, Mar. 2016, pp. 1–6, doi: 10.1109/ICCPCT.2016.7530150.

[35] Z.-L. Gaing, "A particle swarm optimization approach for optimum design of PID controller in AVR system," *IEEE Trans. Energy Convers.*, vol. 19, no. 2, pp. 384–391, Jun. 2004, doi: 10.1109/TEC.2003.821821.

[36] S. Janson and M. Middendorf, "A hierarchical particle swarm optimizer and its adaptive variant," *IEEE Trans. Syst., Man, Cybern. B, Cybern.*, vol. 35, no. 6, pp. 1272–1282, Dec. 2005, doi: 10.1109/TSMCB.2005.850530.

[37] K. Oprzędkiewicz and K. Dziedzic, "A tuning of a fractional order PID controller with the use of particle swarm optimization method," in *Proc. Int. Conf. Artif. Intell. Soft Comput.*, 2017, pp. 394–407.

[38] N. Sadati, M. Zamani, and P. Mohajerin, "Optimum design of fractional order PID for MIMO and SISO systems using particle swarm optimization techniques," in *Proc. IEEE Mechatronics Int. Conf.*, Kumamoto, Japan, May 2007, pp. 1–6, doi: 10.1109/ICMECH.2007.4280056.

[39] S. Das, S. Saha, S. Das, and A. Gupta, "On the selection of tuning methodology of FOPID controllers for the control of higher order processes," *ISA Trans.*, vol. 50, no. 3, pp. 376–388, Jul. 2011.

[40] A. Khurram, H. Rehman, S. Mukhopadhyay, and D. Ali, "Comparative analysis of integer-order and fractional-order proportional integral speed controllers for induction motor drive systems," *J. Power. Electron.*, vol. 18, no. 3, pp. 723–735, 2018, doi: 10.6113/JPE.2018.18.3.723.

[41] K. Sundaravadivu, B. Arun, and K. Saravanan, "Design of fractional order PID controller for liquid level control of spherical tank," in *Proc. IEEE Int. Conf. Control Syst., Comput. Eng.*, Penang, Malaysia, Nov. 2011, pp. 291–295, doi: 10.1109/ICCSCE.2011.6190539.

[42] D. Cafagna, "Fractional calculus: A mathematical tool from the past for present engineers [Past and present]," *IEEE Ind. Electron. Mag.*, vol. 1, no. 2, pp. 35–40, Summer 2007, doi: 10.1109/MIE.2007.901479.

[43] T. Aleksei, P. Eduard, and B. Juri, "A flexible MATLAB tool for optimal fractional-order PID controller design subject to specifications," in *Proc. 31st Chin. Control Conf.*, Hefei, China, 2012, pp. 4698–4703.
[44] A. Tepljakov, "FOMCON: Fractional-order modeling and control toolbox," in *Fractional-order Modeling and Control of Dynamic Systems*. Cham, Switzerland: Springer, 2017, ch. 6, pp. 107–129, doi: 10.1007/978-3-319-52950-9_6.
[45] A. Tepljakov, E. Petlenkov, and J. Belikov, "FOMCON: Fractional-order modeling and control toolbox for MATLAB," *Proc. 18th Int. Conf. Mixed Design Integr. Circuits Syst. (MIXDES)*, Gliwice, Poland, 2011, pp. 684–689.
[46] A. Tepljakov. (2017) *FOMCON: Fractional-Order Modeling and Control. Official Website*. Accessed: Feb. 12, 2021. [Online]. Available: http://fomcon.net
[47] V. Utkin, J. Guldner, and J. Shi, *Sliding Mode Control in Electromechanical Systems*. Philadelphia, PA, USA: Taylor & Francis, 1999.
[48] V. I. Utkin, "Sliding mode control design principles and applications to electric drives," *IEEE Trans. Ind. Electron.*, vol. 40, no. 1, pp. 23–36, Feb. 1993.
[49] C. Wang, Y. Jin, and Y. Chen, "Auto-tuning of FOPI and FO[PI] controllers with iso-damping property," in *Proc. 48th IEEE Conf. Decis. Control (CDC) Held Jointly, 28th Chin. Control Conf.*, Shanghai, China, Dec. 2009, pp. 7309–7314, doi: 10.1109/CDC.2009.5400057.

ATTILA LENDEK (Student Member, IEEE) received the B.S. degree in electrical engineering and the M.S. degree in electrical and computer engineering from Purdue University, Hammond, IN, USA, in 2019 and 2021, respectively.

His research interests include electromagnetism, electrodynamic magnetic levitation, Halbach arrays, magnetic lifting force, finite element analysis, and fractional-order control systems.

LIZHE TAN (Senior Member, IEEE) received the B.S. degree from Southeast University, Nanjing, China, in 1984, and the M.S. degree in engineering mechanics and the M.S. and Ph.D. degrees in electrical engineering from The University of New Mexico, Albuquerque, NM, USA, in 1987, 1989, and 1992, respectively.

He is currently a Professor with the Department of Electrical and Computer Engineering, Purdue University Northwest, Hammond, IN, USA. He has authored or coauthored two textbooks *Digital Signal Processing: Fundamentals and Applications* (Elsevier, Third Edition, 2018) and *Analog Signal Processing and Filter Design* (Linus Publications, Second Edition, 2016). He holds a granted U.S. patent. His research interests include digital adaptive signal processing, control systems, computer vision, robotics, and machine learning. He has served as an Associate Editor for the *International Journal of Engineering Research and Innovation*.